

Powder-Metallurgical Fabrication and Electrical Contact Resistance Characterization of Copper–Nickel Composites Reinforced by Multiwalled Carbon Nanotubes

Daniel García,* Sebastián Suárez,* Katherine Aristizábal, and Frank Mücklich

This article studies copper (Cu)-based composites alloyed with nickel (Ni) and reinforced with carbon nanotubes (CNTs) fabricated via powder metallurgy under pressureless sintering methodology and vacuum. Different compositions of matrices containing 0, 3, and 30 wt% Ni are compared after sintering at 550 and 750 °C. The formation of phases for the different compositions is analyzed by high-temperature X-ray diffraction (HT-XRD) in the solid-state range up to 800 °C, in which reduction of oxides along with the sintering can be identified. Subsequently, the matrices are reinforced with pristine multiwalled CNT (MWCNT) in contents of 0, 0.5, and 1.0 wt% prior to sintering, whose dispersion is influenced by the powder's morphology. A custom-made electrical contact resistance (ECR) setup is used to investigate the electrical behavior of the sintered samples, which, particularly, allows the identification of improvements in electrical conduction of samples containing 0.5 wt% CNT and 3 wt% Ni. A reduction in chemical incompatibilities between Cu and CNT can be attributed to the presence of Ni in solid solution.

1. Introduction

In electrical applications, copper (Cu) and Cu-based alloys stand out among the metals. This is due to the combination of excellent conductivity and affordability.^[1] However, there is a dichotomy associated with Cu and its alloys regarding the compromise between electrical and mechanical properties. On the one hand, it is well known that any type of lattice distortions leads to electron scattering which drastically reduces conductivity and, thus, limits alloying.^[1] On the other hand, the application of high-


purity Cu is restricted by its low strength and its facility for building Kirkendall pores. Adding alumina or silica for particle dispersion strengthening is not a viable option due to their poor conductivities, resulting in an overall increase of the resistivity.^[1,2] The aforementioned dichotomy can be summarized in challenging applications such as electrical contacts. Apart from the need for a wear-resistant contact interface and environmental degradation, it also needs to withstand creep and stress relaxation in the case of deformed joints, as well as thermal expansion and contraction associated with resistive heating.^[3,4]

Despite electron scattering on dispersed particles or secondary phases, studies about the reinforcement of Cu-based metal matrix composites (MMCs) with carbon nanotubes (CNTs) have grown exponentially in the last decade, especially in the fields of micro- and

nanoelectronics for high-power applications requiring thermal stability.^[5] The reasons for using CNT in MMC are manifold: outstanding conductivity as the ballistic electron transport at certain conditions,^[6] superior specific strength,^[2] as well as lubricity^[7] in combination with a low density.^[8] However, achieving a seamless interface between CNT and the metallic matrix is critical as only the composite can benefit from the CNTs' properties.^[5,6,9] Such a challenge has motivated studies aiming at achieving a homogeneous distribution and incorporation of the reinforcement into the metallic matrix on different scale levels. On the macro-scale, CNTs have been used as reinforcements for structures and components in automobiles. Studies conducted by Suárez^[10] and Reinert et al.^[7] reported the reduction of friction and wear by strengthening mechanisms such as grain refinement, hindering of dislocations movement, and sliding. On the micro-scale, they have been used in the manufacturing of microelectromechanical systems (MEMS) with a significant advantage over the conventional silicon (Si) electronics regarding flexibility.^[6] In a novel approach, CNTs have opened nanometer-scale applications such as Y-junctions, electronic gates, and switches.^[6]

Regarding CNT as reinforcement in a Cu matrix, there are three main challenges to be considered. First, a homogeneous dispersion needs to be achieved. This excludes processing techniques such as molten routes due to the risk of agglomeration, segregation, and flammability in the presence of oxygen.^[2,11–13] Aqueous routes, however, have shown positive results regarding dispersion and minimal distortion to the CNT structure via

D. García, S. Suárez, K. Aristizábal, F. Mücklich
Chair of Functional Materials
Department of Materials Science
Saarland University
Saarbrücken D-66123, Germany
E-mail: daniel.garciamunoz@uni-saarland.de;
s.suarez@mx.uni-saarland.de

 The ORCID identification number(s) for the author(s) of this article can be found under <https://doi.org/10.1002/adem.202100755>.

© 2021 The Authors. Advanced Engineering Materials published by Wiley-VCH GmbH. This is an open access article under the terms of the Creative Commons Attribution-NonCommercial-NoDerivs License, which permits use and distribution in any medium, provided the original work is properly cited, the use is non-commercial and no modifications or adaptations are made.

DOI: 10.1002/adem.202100755

electrodeposition. Studies in single-walled CNT^[14] and multi-walled CNTs^[15] have demonstrated the effectiveness of the method, with limitations to film-shaped composites, difficulty to achieve free-standing pieces, and with the assistance of significant functionalization steps. Several studies agree that solid-state processing and powder metallurgy (PM) represent the most feasible route.^[13,16,17] A wide range of parameters can be varied to optimize the process such as the selection of powders with a determined morphology,^[13,17] mixing routes including mechanical milling^[13,17] or sol-gel processing,^[7] temperature, pressure, time, atmosphere, heating, and cooling rates, among others.^[18] Particularly, the use of dendritic and small-sized powders is a strategy also reported to increase the available surface area for CNT entanglement^[13,17]; however, very severe mechanical dispersions can induce damages to the nanotube structure resulting in degradation of the outstanding intrinsic mechanical, electrical, and thermal properties.^[2]

The second challenge in Cu-CNT composites is based on the big differences in surface tension between the metallic matrix (around 1270 mN m⁻¹ for pure Cu^[11]) and reinforcement (between 100–200 mN m⁻¹ for CNT^[11]). Such a different behavior explains the poor wettability as indicated by Doush et al.,^[11] resulting in interfacial discontinuities at the point of producing pores and gaps which hinder the effective mechanical, thermal, and electrical transfer.^[2] Thus, the reinforcement effect is not achieved, and its overall influence results detrimental. Despite having a high surface tension value of nearly 1770 mN m⁻¹,^[19] nickel (Ni) unlike Cu can hold C in dissolution up to 9 at% until reaching saturation.^[20] Such a scenario for the Ni–C interaction offers two bonding possibilities: physisorption and chemisorption. In the former case, the possibility of a strong interaction by charge fluctuations is marginal while in the latter, the interaction is strong, as a result of the overlapping of the outermost C and Ni electrons.^[21] Alloying in small quantities represents a technical solution to improve the properties and overall behavior of Cu, for example, to achieve a greater mechanical response and/or corrosion resistance. However, alloying elements generate also lattice distortions associated with increased scattering of electrons and phonons. The bigger the atomic radii differences between the matrix and alloying elements and/or impurities, the stronger is the scattering effect. In the case of Ni, it has the same face-centered cubic (FCC) crystalline structure as Cu, similar density, and it exhibits complete solubility in the whole range of compositions.^[22–24] In addition, the elastic modulus of Ni will confer its intrinsic higher mechanical properties, chemical resistance, and electrical and thermal resistivity. Because of that,

Ni represents a suitable alloying element for Cu. Moreover, it will generate an associated lattice mismatch of only 2%.^[22,25] Such a difference, however, results in a tripling in electrical conductivity of pure Cu from 0.017 (Ω·mm²) m⁻¹ at 20 °C^[26] to 0.050 (Ω·mm²) m⁻¹ at a concentration as low as 2 wt% Ni, making the alloy suitable for use as resistive heating wires.^[27]

The third challenge in Cu-CNT composites arises from the processing methodology which, as mentioned earlier, relies on the solid-state due to the differences between the matrix and the reinforcement. In the case of powder metallurgy, it offers versatility in all the stages from raw materials processing to sintering atmosphere, generally avoids segregation in most cases, and can be straightforwardly upscaled.^[18] The simplest variant of this process is known as pressureless sintering in which, without the need for external pressure, a good densification and alloy formation can be achieved. In the case of MMCs, it has been reported that the facility for closing pores relies on an optimal dispersion and integration of the reinforcement within the matrix.^[13,17]

During this study, powder metallurgy is used to incorporate CNT as a reinforcement phase into a Cu-based matrix with varying Ni contents. The microstructure of the resulting composite is investigated along with its mechanical response via hardness measurement and electrical behavior. A correlation between optical microscopy findings and electrical contact behavior has been proposed.

2. Results and Discussion

2.1. Powders Characterization

The pristine metal powders were characterized by SEM, as shown in **Figure 1**. In the case of Cu, the flake-shaped particles consisted of tangled, branched, and interconnected dendrites as shown in Figure 1a, exhibiting a smooth appearance, rounded edges, and open porosity. The Ni particles, on the contrary, consist of cauliflower-like dendrites as shown in Figure 1b, exhibiting rough and sharp edges, and growing in branches containing submicrometric features. Both morphologies were purposely selected to guarantee surface entanglement of CNT and it was verified by analyzing a dispersion of Cu powders containing 1.0 wt% CNT after the modified colloidal mixing method, as shown in Figure 1c. Here, a bundle of high aspect ratio CNT can be observed entangled and attached to the surface of a Cu dendritic particle.

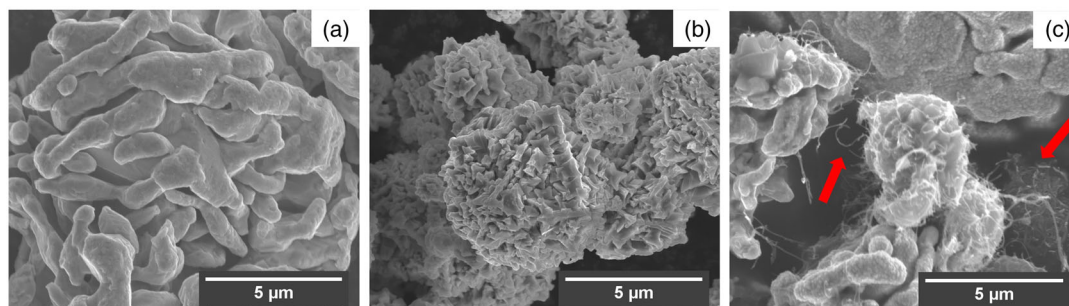


Figure 1. Powders' morphology for a) Cu, b) Ni, and c) Cu with dispersed CNT (pointed by arrows).

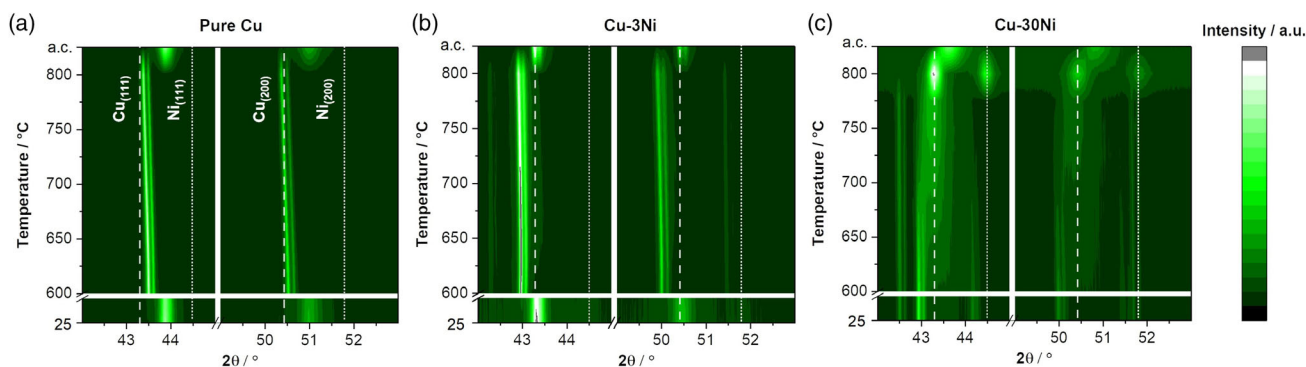


Figure 2. Diffractograms from HT-XRD analysis for the matrices with composition a) Cu, b) Cu–3 wt% Ni, and c) Cu–30 wt% Ni.

2.2. Phase Analysis by HT-XRD

Diffractograms obtained for the different matrices are presented in the form of a contour plot in **Figure 2** with the compositions **(a) Cu**, **(b) Cu–3 wt% Ni**, and **(c) Cu–30 wt% Ni**.

At room temperature, the expected Cu reflections (111) and (200) were visible but shifted from 2θ angles of 43.30° and 50.43° to 43.87° and 50.98° , respectively. These changes, shown in **Figure 2a**, were associated with the lattice strain caused by the compression used to the sample conformation. According to Bragg's equation, such a strain modifies the interplanar distance and shifts the reflection angle. During heating, the position of each reflection was shifted to lower angles as a result of the lattice thermal expansion. In the case of pure Cu, no change in peaks was observed in the studied range and the diffractogram suffered no significant change after cooling.

The addition of Ni, as shown in **Figure 2b**, was hardly noticeable during XRD analysis in samples containing 3 wt% Ni and especially at room temperature. Only the reflection Ni (200) could be identified, weakly and slightly shifted toward a lower angle, while the reflection Ni (100) could not overpass the background noise. In addition to the mechanical distortions, this amount of Ni resulted enough to modify the Cu diffractogram by producing shifting of Cu's main reflections to lower angles than in pure Cu diffractogram. The effect of peaks shifting toward lower angles associated with crystalline lattice expansion was clearly observed during heating. The resolution of Ni peaks was improved during the analysis of samples containing 30 wt% Ni, as shown in **Figure 2c**. Before heating, Ni reflections (111) and (200) were visible near the theoretical 2θ values of 44.5° and 51.8° , they shifted toward lower angles during heating as a result of lattice expansion, and they finally disappeared after cooling by merging with Cu peaks. Here, a transitional merging is observed along with the temperature increase where, considering the whole miscibility of the Cu–Ni system, a single final intermediate peak was expected. However, it ended as a slight unbalance out of the Cu reflections. The reasons for this behavior lie in the incomplete miscibility of Ni into the Cu dominant phase, in which the detected peak distortion is attributed to a lack of holding time at the maximum temperature defined in the HT-XRD analysis.

In **Figure 2b,c**, it is possible to note the presence of a peak located at $2\theta = 42.29^\circ$, especially visible during the high-temperature measurements in the samples containing 30 wt%

Ni. According to studies in superficial oxidation of Cu thin films during annealing,^[28] the corrosion-protective native oxide present in Cu at room temperature can be reduced by thermal activation. Such oxide, exhibiting a diffraction peak at $2\theta = 42.30^\circ$, is associated with the reflection (200) of the cubic phase cuprous oxide (Cu_2O) and it starts to grow at the cost of the Cu reflection (111) when heated in ambient atmosphere. Xiong et al., for example, reported the presence of this peak at $2\theta = 42.39^\circ$ during the synthesis of Cu_2O nanoparticles and indicated that this heat induced growth increases the crystallinity and ordering of the phase, resulting in sharper and narrower XRD peaks.^[29] This argument explains the sharp morphology of the observed peak at $2\theta = 42.50^\circ$ in **Figure 2c**. The slight shifting toward a higher angle can be attributed to internal tensions, arising as a product of the mechanical compression applied.

Temperature and kinetic investigations made by Choudhary et al.^[28] allowed to conclude that the oxide formation rate was particularly increased in the range of $140\text{--}150^\circ\text{C}$, with a significant influence of temperature rather than time due to saturation of the oxide layer and reduction of oxygen diffusion.^[28] Such a finding would explain the presence of the oxide peak in the samples made of powders exposed to EG evaporation in a ventilated furnace at 150°C . This can represent an increase in the electrical resistivity, which is detrimental for applications in electrical contacts. On the contrary, the after-cooling measurements indicated that the oxide peaks were no longer visible and this change was associated with reduction by annealing under a vacuum atmosphere, as reported by Poulston et al.^[30] When heating a CuO substrate above 500°C under a vacuum pressure of $\approx 10^{-6}$ mbar, the regeneration of a fresh metallic Cu layer is possible by O migration from the oxide lattice to the substrate surface.^[30] In the current investigation, the complete loss of the initially reported Cu_2O peak was attributed to this reduction mechanism but under improved kinetics due to the final studied temperature of 800°C . It results worthy to mention that pure Cu samples were not thermally exposed to EG evaporation, and for this reason, the oxide peaks were not detected at this composition.

2.3. Microstructural Characterization

A comparison of the microstructural features found in the different studied mixtures is shown in **Figure 3**.

In general, observations in **Figure 3** show that sintered samples at 550°C present significant decohesion and marked

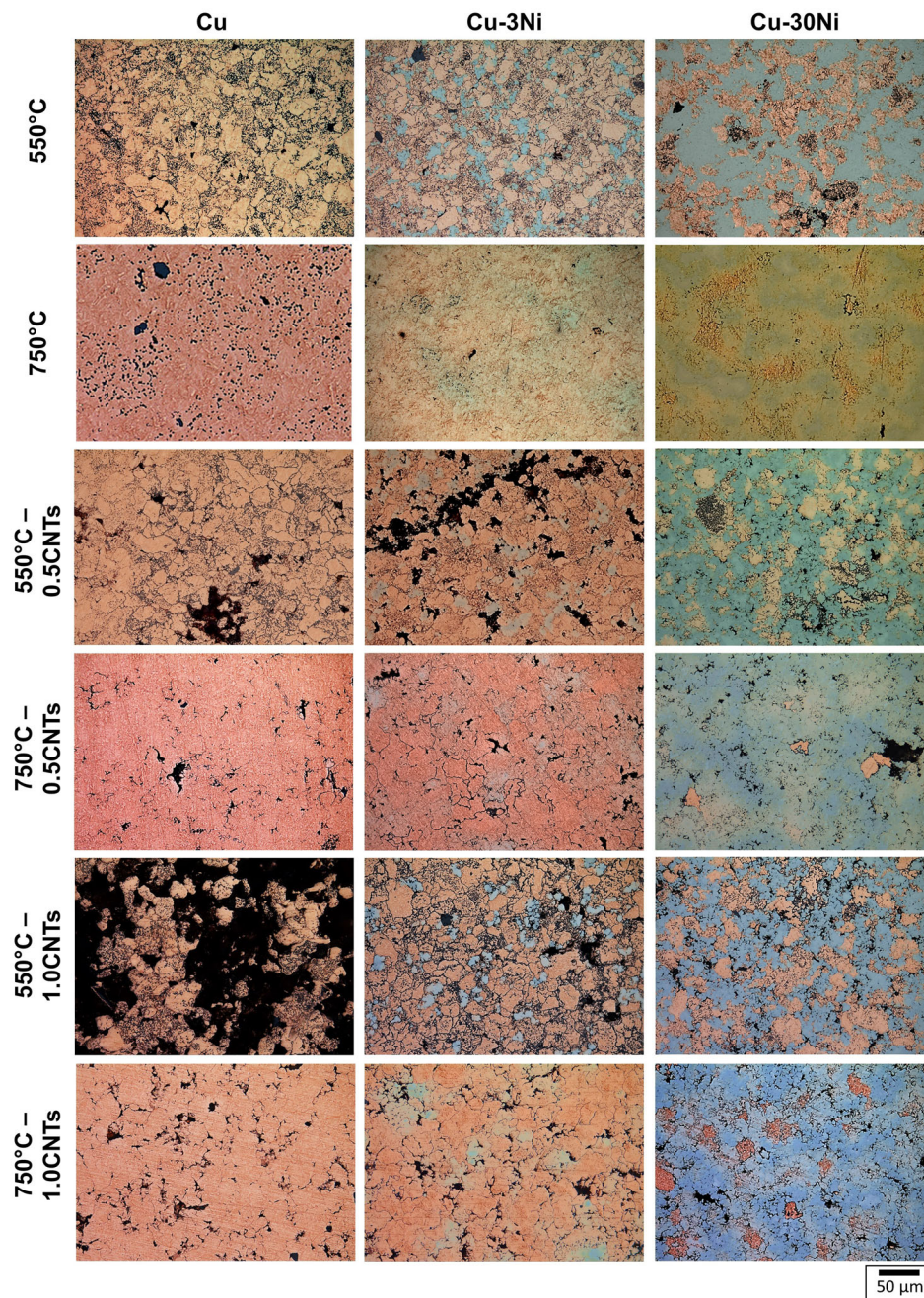


Figure 3. Representative LOM microstructures of studied mixtures with matrix compositions of Cu, Cu–3 wt% Ni, and Cu–30 wt% Ni; reinforcement contents of 0.0 wt% CNT, 0.5 wt% CNT, and 1.0 wt% CNT; sintering temperatures of 550 and 750 °C. Indicated scale bar is valid for all micrographs.

interparticle boundaries, high porosity, and minimal acceptance of CNT in the case of reinforced samples. Details of the observed gaps are assessed in detail afterward during SEM analysis. When comparing the different matrices, the lack of diffusion was a noticeable feature at this temperature, especially visible in the Ni alloyed samples, in which the marked color differences between Cu and Ni allowed the identification of undiffused and homogeneously dispersed alloyant particles. These results are in agreement with the HT-XRD analysis in which the alloy formation is marginal below 600 °C. Unlike Cu, Ni particles were

more sensitive to temperature and they exhibit a better interdiffusion, allowing a more consolidated microstructure. Such a response by the Ni particles exerted an influence on the interfaces with Cu particles, resulting in smoother and more homogeneous boundaries. Despite having a higher melting point than Cu, such an effect of Ni particles was associated with the smaller and refined dendritic structures, as shown in Figure 1.

The samples sintered at 550 °C presented porosity allocated preferentially in the Cu phase. Such a temperature can be considered an activator for the mobility of vacancies which can,

subsequently, coalesce into pores. The resulting pore distribution is not a coincidence, and it can be explained by the intragranular diffusion coefficients. Thus, the diffusion coefficient for Ni in Cu is $(2.6 \times 10^{-6} \text{ cm}^2 \text{ s}^{-1}) \exp(-1.38 \text{ eV} / kT^{-1})$, while in the case for Cu in Ni, the corresponding value is $(5.2 \times 10^{-8} \text{ cm}^2 \text{ s}^{-1}) \exp(-1.51 \text{ eV} / kT^{-1})$.^[31] Initially, Ni atoms will move faster than Cu atoms and a larger vacancy concentration will arise at the Ni-rich side. This vacancy unbalance results in a net flow toward Cu phase and the equilibrium number at the Ni phase is reduced. Such a behavior is especially noticeable in samples containing 30 wt% Ni, in which Cu-rich phase ended plenty of porosity. This fact known as the Kirkendall pore formation explains that once a critical vacancy concentration arises in the Cu-rich side, they will nucleate into pores with a net loss of material as a product of the different diffusion rates.^[32,33]

A detailed analysis of reinforced samples sintered at 550 °C, observed in LOM microstructures of Figure 3, shows that the presence of Ni supports homogeneous CNT dispersion when compared with the unalloyed counterparts and the improvement results proportional to the Ni content. It can be seen, for example, that the sample with composition Cu–1.0 wt% CNT presented critical porosity and reinforcement agglomeration. This fact demonstrates that, despite a physical bonding through EG, the lack of chemical compatibility between matrix and reinforcement predominates at the sintering stage. Thus, the open porosity was associated with partially removed CNT bundles and full removal of nonsintered metallic particles apparently covered by CNT during the polishing step. **Figure 4** shows a detailed view obtained by SEM of samples with composition Cu–1.0 wt% CNT. Without Ni, agglomerates were found to be larger, and they represented a critical barrier against sintering by self-diffusion. At the reinforcement content of 1 wt% CNT, however, samples with matrix composition Cu and Cu–3 wt% Ni exhibited also relatively large agglomerates and open pores.

Sintering at 750 °C evidenced microstructural improvements in the sample densification. In the case of unreinforced matrices, the interparticle boundaries were drastically reduced and, in the case of Ni-alloyed ones, solid solution formation was very close to a single homogeneous phase. Porosity associated with vacancies coalescence was again observed but strongly reduced. For alloyed samples, porosity was preferentially located on Cu-rich zones according to the reddish color of the metal; thus, porosity caused

by different diffusion rates was confirmed. In addition, the individual metallic particles of both metals were hardly differentiable, suggesting ease of mixture at such temperature.

Unlike unreinforced samples, the presence of CNT at the interface between particles represented a clear obstacle for sintering by diffusion mechanisms, being the Cu particles the most affected ones. As an example, let it be considered the LOM microstructure for the composition Cu–3 wt% Ni–0.5 wt% CNT sintered at 750 °C and shown in Figure 3. Despite good homogeneity with mixed Ni particles, some uninfluenced Cu particles were found completely surrounded by CNT. The analysis of reinforced samples with 1.0 wt% CNT sintered at the same temperature confirms the hindering effect for diffusion caused by the reinforcement agglomeration. A preferential distribution around Cu particles can be associated with the difficulty of this metal to store C into its lattice for the generation of a physicochemical binding and, thus, to reduce this type of segregation.^[34]

In summary, densification via pressureless sintering at 550 °C results in a poor thermally activated condition with composites seriously affected microstructurally. The condition of 750 °C offers a significant porosity reduction, as well as a better interparticle bonding, both for unreinforced and reinforced samples. In addition, Ni incorporation to the composite system reduces the risk of CNT allocation around Cu particles during the mass transport occurring during the solid-state sintering. In addition, the highly branched-faceted morphology and the better physicochemical affinity between Ni and C foster homogeneous composite microstructures. Thermal activation promotes vacancy movement which can coalesce into the formation of porosity. The addition of Ni reduces significantly this type of porosity; however, differences in diffusion velocities can nucleate pores in the Cu-rich zones. Reinforcement agglomeration around specific particles can weaken the microstructure, promoting the removal of CNT clusters and even entire isolated undiffused metallic particles.

2.4. Mechanical Behavior

The mechanical behavior of sintered samples was assessed by hardness testing (**Figure 5**). It was possible to note a trend of higher values for samples sintered at 550 °C than those sintered at 750 °C. Despite the microstructural consolidation deficiencies

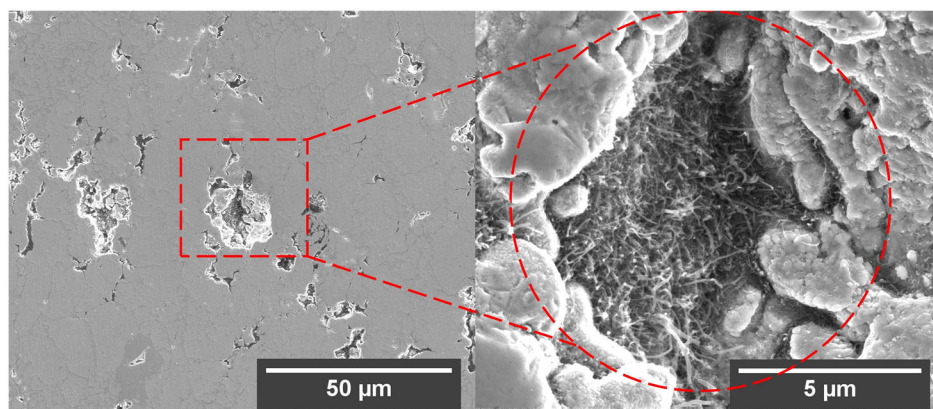


Figure 4. Detail of open porosity in samples with composition Cu–1.0 wt% CNT sintered at 550 °C. A bundle of detached CNT is outlined.

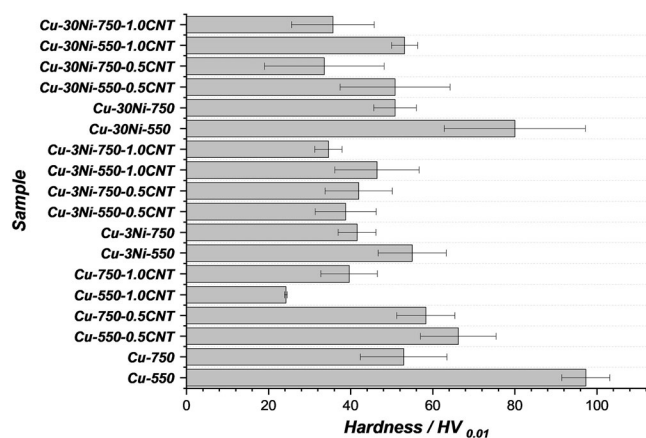


Figure 5. Vickers hardness measurements at an indentation force of 0.01 N.

noted, the reasons behind the observed behavior can be associated with microstructural recovery and grain growth mechanisms occurring at the higher temperature, which make the base metal softer by defects annihilation. Cu samples exhibited a better mechanical behavior which can be associated with the nature of the pristine powder. Adding Ni to the different matrices leads to homogenization effect by reducing the hardness differences between both sintering temperatures. No mechanical improvements were found due to alloy formation in the studied compositions but a tendency to higher hardness values was observed proportional to the Ni content. The presence of reinforcements in a content of 0.5 wt% CNT exhibited a better distribution and integration than those containing 1.0 wt% CNT. The mechanical reinforcement effect was, however, not significant when compared with the unreinforced counterparts. This fact was attributed to the deficiencies in the reinforcement incorporation to the matrix, the introduction of porosity, and decohesion between grains. In the case of the Cu-CNT samples, hardness measurements were difficult to conduct due to the size and number of agglomerates with a significant hardness reduction proportional to the CNT content. Unlike unalloyed samples, the presence of Ni evidenced a better integration of CNT with an improvement in the mechanical characteristics.

2.5. Electrical Measurements

Results for ECR are shown in **Figure 6**, grouped into different matrix compositions. An analysis of the standard error indicates that, apart from some few outliers, the error average is below 25%. Each curve consists of loading (1) and unloading (2) stages, going from 1 to 10 N and back to 1 N, respectively. In the first stage, the resistance decreased with the increasing load until reaching saturation in the second stage, and finally, a resistance recovery was observed lying below the initial path. The value of the ECR is, as stated by Slade,^[33] directly proportional to the square root of the ratio between the indentation hardness and the applied normal load. This behavior arises as a result of the mechanical interaction between the hemispherical tip and the contact surface features (asperities), the rupture of thin

contaminant surface films (of oxidic and/or organic nature), and a continuous increase of the real contact area resulting from the deformation of topographical features. These deformations can be classified into two categories, namely, plastic and elastic, which have a direct influence on the ECR value. The different slope changes observed on the curves along with the increase in the applied load can be associated with the transition from an elastic to plastic deformation regime, while the noted resistance increase during the unloading cycle (clearly lower in magnitude when compared with the loading cycle) is associated with a reduction of the real contact area.

Results for unalloyed Cu without and with reinforcements are shown in Figure 6a. It can be noted that unreinforced pure Cu sintered at both studied temperatures offer similar and one of the lowest ECR values at the unloading force of 9 N, being the values 10.46 mΩ for 550 °C and 15.22 mΩ for 750 °C. For the same unalloyed matrix, the addition of CNT resulted in a general increase of ECR and, in agreement with microstructural findings, sintered samples at 750 °C presented lower ECR values when compared with the counterparts sintered at 550 °C. Regarding the reinforcement electrical effect, the amount of 1.0 wt% CNT resulted in a final lower ECR value than 0.5 wt% CNT, suggesting that this kind of reinforcement exerts an electrical improvement. It is known that an ineffective interaction at the Cu-C interphase in addition to dispersion inhomogeneities has a detrimental effect on the good electrical behavior of pure Cu due to electron scattering. This explains why unreinforced Cu could not be surpassed in conductivity; however, it results worthy to mention that despite the observed defects, the composites managed to be within the same order of magnitude.

Results for matrices with composition Cu-3 wt% Ni without and with reinforcements are shown in Figure 6b. From the graph, it can be noted that the presence of Ni raised the ECR to nearly one order of magnitude when compared with the pure Cu samples. In the particular case of unreinforced samples sintered at 750 °C, the minimum ECR value was found to be higher than the one of samples sintered at 550 °C. This fact indicates that alloy formation might be more detrimental to electron scattering than having dispersed undiffused Ni particles, as evidenced in the LOM analysis. This situation was, however, reversed after the incorporation of CNT in which the reinforced samples exhibited a better electrical behavior than the unreinforced counterparts. The sintering condition of 750 °C showed an enhanced electrical behavior, reaching a minimum value of 9.29 mΩ in samples containing 0.5 wt% CNT. This value is even lower than those measured for pure Cu. There are two possible explanations for this. The first one is related to the better chemical compatibility between Ni and C, allowing an improved interface between the solid solution matrix and the reinforcement. The second one considers the improved CNT dispersion reached under the presence of Ni particles in which smaller and better dispersed agglomerates were detected. Thus, small additions of Ni act as a bridge for the right coupling of CNT and a partial transfer of their outstanding electrical properties can be achieved. In addition, a similar trend regarding matrix homogenization was observed in samples containing 1.0 wt% CNT, reaching a better electrical performance those sintered at 750 °C than the ones at 550 °C. Despite the higher CNT content,

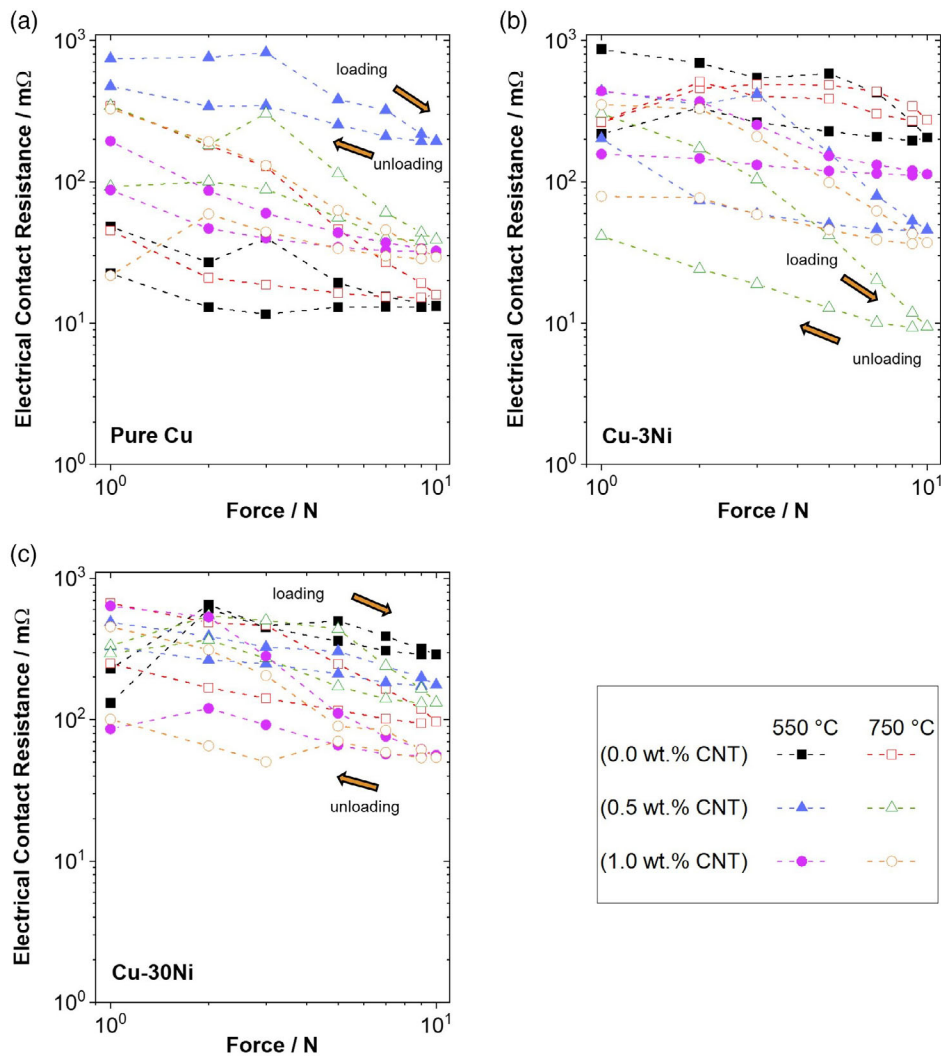


Figure 6. ECR comparison in different reinforcement content and sintering temperatures for matrices with composition a) Cu, b) Cu-3 wt% Ni, and c) Cu-30 wt% Ni. Loading and unloading stages are depicted in the graphs. Error bars were omitted for a better understanding of the graphs.

samples containing 1.0 wt% CNT could not perform electrically better than those containing 0.5 wt% CNT.

Finally, results for matrices with composition Cu-30 wt% Ni without and with reinforcements are shown in Figure 6c. A higher Ni content resulted in ECR values clearly above one order of magnitude when compared with pure Cu samples. The possibility of having remanent Cu oxides, as detected during the XRD analysis, should also be considered in this stage as a cause for the significant resistance increase. The electrical influence of the reinforcement becomes more evident in this composition. It can be noted that the electrical performance was improved for samples containing 1.0 wt% CNT, reaching a minimum ECR value of 53.57 mΩ at an unloading force of 9 N for samples sintered at 750 °C. The reasons for such behavior, in which the higher CNT content produced an overall better electrical response, are supported by the fact that Ni is a better C acceptor in the Cu-Ni system.^[34] In addition, a trend for slightly lower ECR values in samples with lower hardness and those

sintered at 750 °C is observed and can be associated with two possible reasons. The first one is attributed to the existent proportionality between ECR and the square root of the hardness, as indicated by Slade.^[33] The second reason lays in more compact microstructures in which less porosity and fewer interparticle boundaries associated with electron scattering were observed.

3. Conclusions

The effect on the electrical behavior of Cu and Cu-Ni matrix-based CNT-reinforced composites processed via PM was studied in this work. According to the literature, any distortion to the crystalline lattice of pure Cu produces electron scattering and its outstanding conductivity is affected. Reinforcements are not an exception and, in the case of CNT, an optimal coupling between the interface and the reinforcement must be guaranteed to transfer their exceptional properties. Despite the known chemical incompatibilities between Cu and C, the strategy assessed in

this work managed to equalize and even improve the electrical behavior of the processed MMCs by adding small amounts of Ni. This addition, together with sintering at 750 °C, derived in more homogeneous microstructures, porosity reduction compared with the unalloyed counterparts, and resulted in improved reinforcement dispersion as observed in the LOM analysis. Such effects were attributed to the physicochemical similarities with Cu and better affinity with C. Regarding the reinforcement effect, the addition of 1.0 wt% CNT resulted in lower ECR values for matrix groups with composition Cu and Cu–30 wt% Ni. In the case of samples containing 3 wt% Ni, the optimal reinforcement content for reducing ECR, even below Cu values, was found to be 0.5 wt% CNT for samples sintered at 750 °C. Notably, CNT dispersion represents an additional challenging step with microstructural and electrical implications; however, the selection of dendritic powders produced an improved acceptance of the reinforcement by entanglement at the surface of the metallic particles. From the studied sintering temperatures, a general better electrical response was observed in samples sintered at 750 °C than those at 550 °C. Reasons for such a behavior lie in the better formation of solid solution detected in XRD measurements with an effect on microstructural homogeneity. Pressureless sintering resulted hardly enough for the consolidation of the samples, but it did not allow mechanical improvements after the incorporation of reinforcement and/or alloyant. Finally, the results obtained during this study contribute to an improved understanding of sintering mechanisms for dissimilar materials driven by vacancies diffusion and concentration gradients.

4. Experimental Section

The studied systems were Cu-based composites with three different Ni contents: 0, 3, and 30 wt% Ni. Each matrix composition was reinforced with either 0, 0.5, or 1.0 wt% of CNT.

Cu powder (Alfa Aesar GmbH & Co KG, 325 mesh, 99% purity) and Ni dendritic powder (Alfa Aesar GmbH & Co KG, 325 mesh, 99.8% purity) were selected as matrix materials. The powders were blended through a colloidal mixing method,^[7] consisting of powders dispersion in ethylene glycol (EG) and subsequent homogenization by shear mixing (Ultra-Turrax T-25 by IKA) at 7000 rpm for 10 min. To avoid precipitation of the powders in EG, a ratio of 0.25 g mL⁻¹ was preserved. The reinforcement consisted of multiwalled carbon nanotubes (MWCNTs) (CCVD grown, Graphene supermarket, USA, diameter 50–85 nm, length 10–15 μm, carbon purity >94%). Similar to the metallic powders, MWCNTs were dispersed in EG via a modified colloidal mixing method which includes dispersion in a shear mixer for 10 min, while a ratio CNT/EG of 0.2 mg mL⁻¹ is preserved.^[35] Afterward, the suspension was sonicated for 20 min (Sonorex Super RK 514 BH by Badelin, 860 W, 35 kHz). This sonication time guarantees proper disentanglement with no significant CNT structural damage.^[36,37] Next, both suspensions were mixed in a shear mixer for 10 min. Finally, the mixed suspensions were dried in a ventilated laboratory stove at 150 °C for 8 h.

Fabrication of cylindrical-shaped samples with roughly 3 mm in height was achieved by pressing the different powder mixtures in a cylindrical steel die with 8 mm in diameter at a normal pressure of 1300 MPa. Sample sintering was performed in a pressureless arrangement at 550 and 750 °C in a tubular vacuum oven with a working pressure of 10⁻⁶ bar, a heating rate of 1 (°C) min⁻¹, and an isothermal holding time of 2.5 h. Cooling was performed inside the oven until reaching a minimum of 100 °C. For statistical considerations, each composition was fabricated in triplicate. Regarding the metallographic preparation, sintered samples were embedded in a conductive thermoset resin, grounded under water

rinsing in an automatic grinding machine (TegraPol-21, by Struers, 20 N force, speed 150 rpm), with successive sandpaper grit sizes of 320, 600, 1200, 2500, and subsequently polishing using diamond suspensions of 6, 3, 1 μm, and chemical etching with oxide polishing suspension (OPS).

The initial powders' morphology was verified by scanning electron microscopy (SEM) (Helios NanoLab600, FEI), as well as the morphology of the particles after the reinforcement dispersion. Phase analysis was conducted by performing high-temperature X-ray diffraction (HT-XRD) (PANalytical X'Pert Pro MPD, PANalytical) under Bragg–Brentano geometry and with Cu Kα radiation of wavelength $\lambda_{Cu} = 1.540598 \text{ \AA}$. A fixed angle divergence slit of 0.5° and a HT-sintering chamber (Anton Paar HTK1200) at 10⁻⁶ mbar were also coupled to the arrangement. Measurements were initially performed at room temperature with subsequent measurements in a range of 600–800 °C at intervals of 25 °C. The scanning range 2θ was selected between 42° and 53° to follow the first two most intense reflections during the sintering cycle. The step size was defined as 0.013° and a time per step of 68.595 s. The acceleration voltage and current employed were 40 kV and 40 mA, respectively.

Complementary to SEM, light optical microscopy (LOM) was performed with a Leica DM 6000 M (Leica Microsystems). The mechanical response of the sintered samples was studied by Vickers hardness measurements (Struers Dura Scan 50, Struers Inc.) at a force of 0.01 N with six indentations per sample on the polished side. Finally, the electrical contact resistance (ECR) was measured on the polished side of the sample. For this measurement, the sample was degreased by ultrasonically washing in acetone, isopropanol, and ethanol, and then fixed with silver (Ag) ink onto a Cu foil coated with tin (Sn) film which worked as a sample holder. The sample was approached against a AuCo_{0.2}-coated hemispherical rivet (Adam Bornbaum GmbH) via a piezo-stage and pressed with loading forces of 1, 2, 3, 5, 7, 9, and 10 N. The unloading cycle followed the same force steps. At each load, a series of 5 electrical measurements at a maximum current of 0.1 A were performed in three different surface sites each, in which the voltage drop was measured, and the resistance was calculated. To avoid human influence and ensure repeatability during operation, the loading and electrical measurements were operated through a custom-made LabView program.

Acknowledgements

The authors gratefully acknowledge funding in the ZuMat project, supported by the State of Saarland from the European Regional Development Fund (Europäischen Fonds für Regionale Entwicklung, EFRE).

Open access funding enabled and organized by Projekt DEAL.

Conflict of Interest

The authors declare no conflict of interest.

Data Availability Statement

Research data are not shared.

Keywords

electrical properties, metal matrix composites, nanostructures, powder metallurgy

Received: June 16, 2021

Revised: August 4, 2021

Published online: September 21, 2021

- [1] H.-J. Bargel, G. Schulze, *Werkstoffkunde*, Springer-Verlag, Berlin **2005**.
- [2] S. Zhao, Z. Zheng, Z. Huang, S. Dong, P. Luo, Z. Zhang, Y. Wang, *Mater. Sci. Eng. A* **2016**, 675, 82.
- [3] D. Chapman, H. W. Turner, C. Turner, Copper Development Association **2015**, p. 40.
- [4] G. Kulwanoski, M. Gaynes, A. Smith, B. Darrow, in *Electrical Contacts - 1991 Proc. of the Thirty-Seventh IEEE HOLM Conf. on Electrical Contacts*, IEEE, Chicago **1991**, p. 184.
- [5] R. M. Sundaram, A. Sekiguchi, M. Sekiya, T. Yamada, K. Hata, *R. Soc. Open Sci.* **2018**, 5, 180814.
- [6] P. R. Bandaru, *J. Nanosci. Nanotechnol.* **2007**, 7, 1239.
- [7] L. Reinert, I. Green, S. Gimmmler, B. Lechthaler, F. Mücklich, S. Suárez, *Wear* **2018**, 408–409, 72.
- [8] C. Laurent, E. Flahaut, A. Peigney, *Carbon* **2010**, 48, 2994.
- [9] T. Michel, M. Paillet, P. Poncharal, A. Zahab, J. L. Sauvajol, J. C. Meyer, S. Roth, *Carbon Nanotubes: From Basic Research To Nanotechnology*, Springer Verlag, The Netherlands **2005**.
- [10] S. Suárez Vallejo, Development of Carbon Nanotube-Reinforced Nickel Matrix Composites: Processing, Microstructure and Physical Properties, Universität des Saarlandes, **2014**.
- [11] W. M. Daoush, B. K. Lim, C. B. Mo, D. H. Nam, S. H. Hong, *Mater. Sci. Eng. A* **2009**, 513–514, 247.
- [12] V. Georgakilas, D. Gournis, V. Tzitzios, L. Pasquato, D. M. Guldi, M. Prato, *J. Mater. Chem.* **2007**, 17, 2679.
- [13] S. M. Uddin, T. Mahmud, C. Wolf, C. Glanz, I. Kolaric, C. Volkmer, H. Höllner, U. Wienecke, S. Roth, H. J. Fecht, *Compos. Sci. Technol.* **2010**, 70, 2253.
- [14] P. M. V. Raja, G. L. Esquenazi, C. E. Gowenlock, D. R. Jones, J. Li, B. Brinson, A. R. Barron, *C* **2019**, 5, 14.
- [15] S. Arai, T. Saito, M. Endo, *J. Electrochem. Soc.* **2010**, 157, 147.
- [16] C. Kim, B. Lim, B. Kim, U. Shim, S. Oh, B. Sung, J. Choi, J. Ki, S. Baik, *Synth. Met.* **2009**, 159, 424.
- [17] S. El-Khatib, A. Y. Shash, A. El-Habak, A. H. Elsayed, *Materwiss. Werkstofftech.* **2019**, 50, 588.
- [18] S.-J. L. Kang, *Sintering: Densification, Grain Growth, and Microstructure*, Elsevier Ltd, Oxford **2005**.
- [19] J. Brillo, I. Egry, *J. Mater. Sci.* **2005**, 40, 2213.
- [20] D. Bandyopadhyay, P. C. Sharma, N. Chakraborti, *J. Phase Equilib.* **2000**, 21, 186.
- [21] J. Tao, H. Tang, A. Patra, P. Bhattarai, J. P. Perdew, *Phys. Rev. B* **2018**, 97, 165403.
- [22] C. R. Brooks, *Heat Treatment, Structure, and Properties of Nonferrous Alloys*, ASM International, Ohio **1982**.
- [23] R. E. Reed-Hill, L. Abbaschian, R. Abbaschian, *Physical Metallurgy Principles*, Cengage Learning, Stamford **2009**.
- [24] W. D. Callister, *Materials Science And Engineering: An Introduction*, John Wiley & Sons, Inc., USA **2007**.
- [25] M. B. M. N. Abdul, S. Yokoyama, *Mater. Trans.* **2017**, 58, 11.
- [26] Department of commerce of the United States, Circular of the Bureau of Standards **1914**, 31, p. 76.
- [27] ASTM International, ASTM B267-07(2018) Standard Specification for Wire for Use in Wire-Wound Resistors, **2018**.
- [28] S. Choudhary, J. V. N. Sarma, S. Pande, S. Ababou-Girard, P. Turban, B. Lepine, S. Gangopadhyay, *AIP Adv.* **2018**, 8, 1.
- [29] L. Xiong, H. Xiao, S. Chen, Z. Chen, X. Yi, S. Wen, G. Zheng, Y. Ding, H. Yu, *RSC Adv.* **2014**, 4, 62115.
- [30] S. Poulston, P. M. Parlett, P. Stone, M. Bowker, *Surf. Interface Anal.* **1996**, 24, 811.
- [31] B. C. Johnson, C. L. Bauer, A. G. Jordan, *J. Appl. Phys.* **1986**, 59, 1147.
- [32] I. D. Choi, D. K. Matlock, D. L. Olson, *Mater. Sci. Eng. A* **1990**, 124.
- [33] P. G. Slade, *Electrical Contacts: Principles and Applications*, CRC Press, USA **2014**.
- [34] A. Agarwal, S. R. Bakshi, D. Lahiri, *Carbon Nanotubes: Reinforced Metal Matrix Composites*, CRC Press, Boca Raton, FL, USA **2016**.
- [35] K. Aristizabal, A. Katzensteiner, A. Bachmaier, F. Mücklich, S. Suarez, *Carbon* **2017**, 125, 156.
- [36] S. Suarez, F. Lasserre, O. Prat, F. Mücklich, *Phys. Status Solidi Appl. Mater. Sci.* **2014**, 211, 1555.
- [37] L. Reinert, M. Zeiger, S. Suárez, V. Presser, F. Mücklich, *RSC Adv.* **2015**, 5, 95149.